

# Morphology-Controllable Ultrafast Fiber Lasers Based on Intracavity Manipulation of Transverse Modes

Heze Zhang, Yang Zheng, Dong Mao<sup>✉</sup>, \* Chao Zeng, Yueqing Du, and Jianlin Zhao

*Key Laboratory of Light Field Manipulation and Information Acquisition, Ministry of Industry and Information Technology, Shaanxi Key Laboratory of Optical Information Technology, School of Physical Science and Technology, Northwestern Polytechnical University, Xi'an 710129, China*



(Received 14 July 2021; revised 7 September 2021; accepted 9 September 2021; published 27 September 2021)

The performances of mode-locked fiber lasers rest with the design and configuration of the cavity, and their temporal morphologies are rarely linked with the modulation of transverse modes. Here, we demonstrate a morphology-controllable ultrafast fiber laser based on the intracavity manipulation of transverse modes, capable of producing dual-color pulses, narrowband picosecond pulses, and broadband femtosecond pulses. Unlike traditional multicolor pulses with unequal group velocities, the dual-color pulse operates in a synchronous state, displaying a multipulse structure where the modulation period relies on the group-delay difference of two modes in the fiber. Simulation results fully reproduce the experimental observations and show that the laser follows the minimum-loss principle with pulse morphologies depending on the mode-interference-induced filtering effect. This work connects transverse-mode modulation with pulse morphology, providing a stable and cost-effective laser source for terahertz-wave generation and nonlinear spectroscopy.

DOI: 10.1103/PhysRevApplied.16.034045

## I. INTRODUCTION

Mode-locked fiber lasers have brought a huge impact on fundamental research and practical applications due to their inherent advantages of cost-effectiveness, compact structure, excellent beam quality, and high reliability [1–4]. The performances of mode-locked fiber lasers hinge on the configuration and parameters of the cavity [5]. By trimming the cavity dispersion from anomalous to normal, conventional solitons [6,7], stretched pulses [8,9], self-similar pulses [10,11], and dissipative solitons [12,13] are achieved in ultrafast single-mode fiber (SMF) lasers. These pulses have durations of femtoseconds to picoseconds with bandwidths spanning from the sub-nanometer region to tens of nanometers [14,15]. Based on the cavity-filtering effect or two-humped gain spectrum, dual-color conventional solitons [16,17] and dissipative solitons [18–20] are realized in erbium-doped fiber lasers and thulium-doped fiber lasers, respectively. Influenced by the group-delay dispersion of the resonator, these dual-color solitons propagate at different group velocities, evolving independently and colliding periodically inside the cavity [21,22]. The spectrum of dual-color solitons mainly depends on the gain profile or cavity-filtering effect, and the pulse is difficult to synchronize in the time domain.

Currently, multimode fiber lasers and few-mode fiber (FMF) lasers are attracting increasing interest due to their

diverse spatial-mode properties [23,24]. Via the counteraction of the intermodal and chromatic dispersions with strong spatial and spectral-filtering effects, spatiotemporal mode-locking operations are demonstrated in multimode fiber lasers, producing picosecond-to-femtosecond optical fields composed of multiple transverse modes with energies up to 150 nJ [25–27]. Furthermore, based on long-period fiber gratings (LPFGs) and mode-selective couplers, cylindrical vector beams and vortex beams are achieved by modulating the transverse modes in hybrid-structure SMF-FMF lasers [28–31]. Nonetheless, the manipulation of transverse modes is rarely linked with the control of pulse morphology, and the hybrid-structure fiber lasers usually emit single-type mode-locked pulses.

As the two-mode fiber (TMF) supports LP<sub>01</sub> and LP<sub>11</sub> modes with unequal propagation constants (i.e., intermodal dispersion), it can introduce an optical-path difference proportional to the fiber length [32]. Thus, a comblike spectral filter with tunable modulation depth and period can be realized by controlling the intensity ratio of the LP<sub>01</sub> and LP<sub>11</sub> modes and fiber length. Based on a controllable mode-interference-induced filter (MIIF), we demonstrate a multifunctional ultrafast fiber laser capable of producing dual-color synchronized pulses, narrowband picosecond pulses, and broadband femtosecond pulses. Remarkably, the frequency difference of two spectra, equaling the repetition rate of a subpulse in the envelope, relies on the TMF length and can be tuned from 0.33 to 0.51 THz. The laser operation follows a minimum-loss principle that the pulse

\*maodong@nwpu.edu.cn

morphology relies on the mode-interference-induced filtering effect. For example, the saturable absorber drives dual-color pulses into a synchronous status, despite the small residual group-delay dispersion of the cavity. This work not only connects transverse-mode modulation with pulse morphology, but also provides a multifunctional laser source for fundamental research and practical applications.

## II. PRINCIPLE AND EXPERIMENTAL SETUP

The setup of the morphology-controllable ultrafast fiber laser is shown in Fig. 1(a), in which the 3.5-m erbium-doped fiber (EDF, Nufern EDL-980-HP) is pumped by a 980-nm laser diode (LD) through a 980/1550-nm wavelength division multiplexer (WDM). In a single round trip, the laser is amplified by the gain fiber, and then subsequently passes through an output coupler (OC), a carbon-nanotube saturable absorber (CNT SA), an inline polarization controller (PC), a MIIF with a TMF (OFS, two-mode step-index fiber) length of 1.5 m and a polarization-insensitive isolator (PIISO). The PC introduces squeezing and twisting on the fiber, which can tune the polarization state to optimize the mode-locking state. The other fiber is a standard single-mode fiber (Corning, SMF-28e+), giving a total length and net dispersion of 8.22 m and  $-0.014 \text{ ps}^2$ , respectively.

The configuration of the MIIF is shown in Fig. 1(b), which consists of a section of step-index TMF, a pressure-induced LPFG, and two sections of SMFs. When light enters from the SMF into the TMF, part of the LP<sub>01</sub> mode couples to the LP<sub>11</sub> mode with the assistance of the LPFG, in which refractive-index modulation can be controlled by pressure [33–36]. After propagation through the TMF, a phase difference between two modes is introduced due to

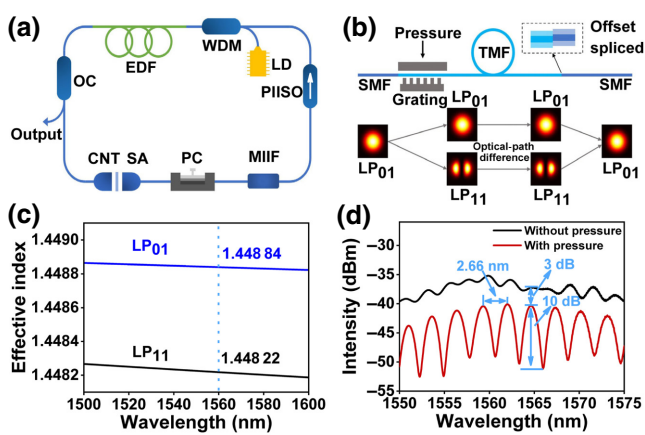


FIG. 1. Principle and experimental setup of morphology-controllable ultrafast fiber lasers. (a) Configuration of the fiber laser. (b) Principle of the MIIF. (c) Effective refractive indices of LP<sub>01</sub> and LP<sub>11</sub> modes in TMF. (d) Performance of MIIF without (black curve) and with (red curve) pressure on TMF.

intermodal dispersion of the TMF. At the output terminal, the TMF and SMF are offset spliced, in which two modes interfere with each other at the connection point. Thus, the spectral intensity is periodically modulated with respect to the wavelength,  $\lambda$ :

$$I = I_1 + I_2 + 2\sqrt{I_1 I_2} \cos(2\pi \Delta n_{\text{eff}} L / \lambda). \quad (1)$$

Here,  $I_1$  and  $I_2$  are the intensities of the LP<sub>01</sub> and LP<sub>11</sub> modes, respectively;  $\Delta n_{\text{eff}}$  is the effective refractive-index difference between two modes; and  $L$  is the length of the TMF. The modulation period of the filter can be approximated as [37]

$$\Delta\lambda \approx \lambda^2 / \Delta n_{\text{eff}} L. \quad (2)$$

It can be seen from Eqs. (1) and (2) that the modulation depth depends on the intensity ratio between two modes, while the modulation period relates to the TMF length. Thus, the spectral-filtering effect can be introduced or eliminated by controlling the intensity ratio between two modes.

Based on the experimental parameters of the TMF,  $\Delta n_{\text{eff}}$  is calculated to be  $6.2 \times 10^{-4}$  at 1560 nm [Fig. 1(c)]. Before imparting pressure on the TMF, only an ignorable part of the LP<sub>01</sub> mode couples to the LP<sub>11</sub> mode and the spectral-filtering effect can be neglected. When pressure is applied on the TMF, the LPFG converts part of the LP<sub>01</sub> mode to the LP<sub>11</sub> mode and they interfere in the SMF. Figure 1(d) shows the transmission spectrum of the filter before and after imposing pressure on the TMF. For the 1.5-m TMF, the filter has a modulation period of 2.66 nm with a maximal extinction ratio of 10 dB and an extra loss of 3 dB.

## III. EXPERIMENTAL RESULTS

With the assistance of the MIIF, we first achieve a dual-color synchronized mode-locked laser in the near-zero dispersion regime. Figure 2(a) shows the typical spectrum of the dual-color pulse for a TMF length of 1.5 m and pump power of 19.4 mW, which comprises two separated spectra at 1558.63 and 1561.32 nm with bandwidths of 0.39 and 0.37 nm, respectively. Attributed to the intracavity four-wave mixing effect, two lower subspectra at 1555.95 and 1564.06 nm always accompany the dual-color mode-locked spectrum. Unlike other dual-color mode locking where two pulses emit at different repetition rates, the dual-color pulse here circulates at the same repetition rate of 25.04 MHz with a signal-to-noise ratio of 67 dB [Fig. 2(b)].

In a single round trip, only one pulse is observed on the oscilloscope [Fig. 2(c)], confirming that the dual-color laser operates in the stable synchronous state. The separation of neighboring pulses is 40 ns, which is consistent with

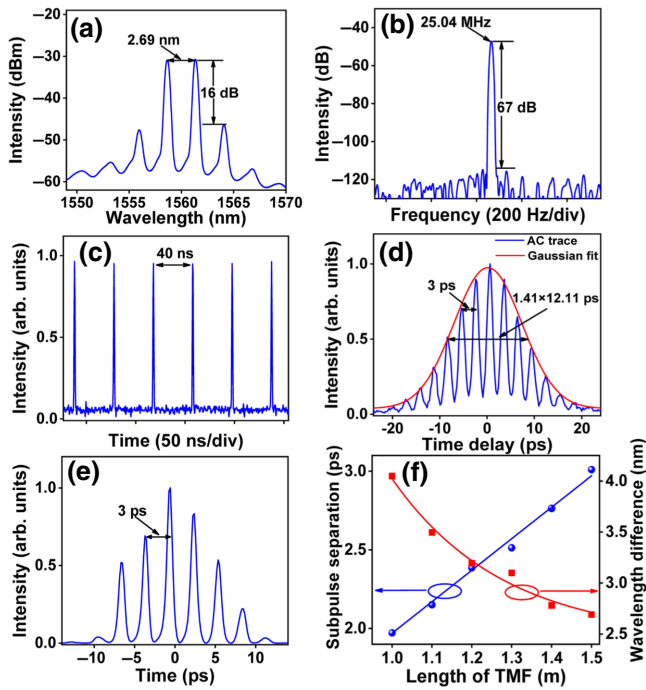


FIG. 2. Performance of dual-color synchronized pulses. (a) Spectrum; (b) radio-frequency spectrum; (c) pulse train; (d) AC trace; (e) retrieved pulse profile from FROG trace; (f) subpulse separation and wavelength difference versus TMF length.

the 8.22-m cavity length. The autocorrelation (AC) trace [Fig. 2(d)] displays a multipeak structure, giving an envelope width of 12.11 ps by Gaussian fitting. The separation of neighboring subpulses is 3 ps, which equals the group-delay difference of two modes accumulated in the TMF. The subpulse repetition rates are calculated to be 0.33 THz, which agrees well with the frequency difference between two central wavelengths of the spectrum. The pulse profile [Fig. 2(e)] retrieved from the frequency-resolved optic gating (FROG) trace (see Part 1 of the Supplemental Material [38]) exhibits a periodically modulated fine structure and fully coincides with the measured AC trace [Fig. 2(d)].

As described by Eq. (2), the modulation period of the MIIF relies on the length of the TMF. By decreasing the length of the TMF from 1.5 to 1 m, with a step of 0.1 m, similar dual-color synchronized pulses can also be obtained in the proposed fiber laser (see Part 2 of the Supplemental Material [38]). One can observe from Fig. 2(f) that the subpulse separation is linearly proportional to the length of the TMF, related by 2.1 ps/m, which is equal to the group-delay difference of two modes. The reciprocal relationship between wavelength separation and TMF length is also consistent with MIIF theory. In the aforementioned cases, the two spectra possess the same polarization state, i.e., scalar dual-color synchronized pulses. Nonetheless, at certain PC settings, vector dual-color synchronized pulses are also observed, in which

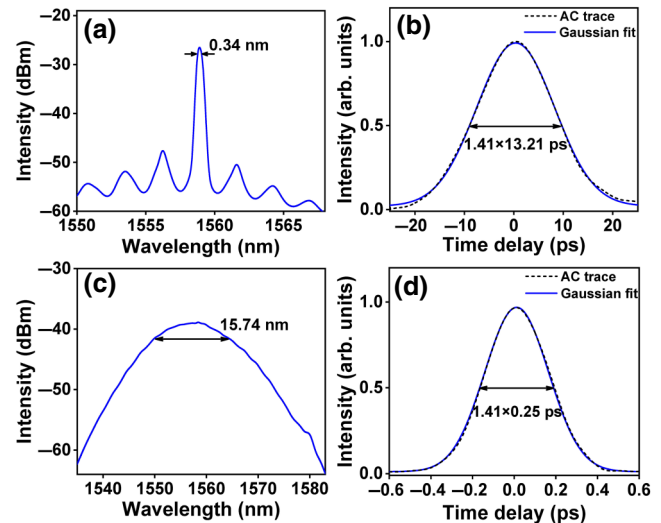


FIG. 3. Properties of narrowband pulses and broadband stretched pulses. (a),(c) Typical output spectrum; (b),(d) AC trace of output pulse.

the two spectra are quasi-orthogonally polarized and the subspectra almost vanish (see Part 3 of the Supplemental Material [38]). However, the vector operation is less stable and can be easily transformed into the scalar state under environmental disturbance, which results from the polarization-insensitive saturable absorption effect as the scalar pulse has a higher instantaneous power than that of the vector one.

Since the EDF exhibits an uneven gain spectrum, the transmission peak of the MIIF can be tuned to the maximum gain by slightly stretching the TMF, and then a narrowband mode-locked pulse will be achieved with the assistance of the PC. As shown in Fig. 3(a), the spectrum displays periodic modulation on the pedestal, with a central wavelength of 1558.91 nm and 3-dB bandwidth of 0.34 nm. The output pulse has a duration of 13.21 ps, which is comparable with the envelope width of the dual-color synchronized pulse, as shown in Fig. 3(b). The time-bandwidth product is calculated to be 0.56, indicating a slightly chirped pulse. In a single period of the MIIF, the spectral center can be continuously increased from 1561 to 1565 nm by further stretching the TMF (see Part 4 of the Supplemental Material [38]), indicating a feasible tunability of the lasing wavelength.

By removing pressure from the TMF, the energy of the LP<sub>11</sub> mode is negligible and the spectral-filtering effect vanishes. In this operation, the fiber laser can be regarded as a typical dispersion-managed fiber laser, enabling the generation of a broadband stretched pulse. As shown in Figs. 3(c) and 3(d), its bandwidth and duration are given as 15.74 nm and 0.25 ps, respectively. The time-bandwidth product is calculated to be 0.49, which is quite close to

that of the chirp-free pulses. In the two states, only a single pulse circulates in the cavity and the pulse interval is the same as that of the dual-color mode-locked pulse. As depicted in Figs. S1(c) and S1(d) within the Supplemental Material [38], the signal-to-noise ratios are given as 67 and 71 dB for the narrowband pulse and the broadband pulse, respectively, confirming the good stability of mode-locked lasers. The aforementioned results indicate that the pulse morphology can be simply controlled by manipulating the coupling behavior of two transverse modes in the MIIF.

#### IV. SIMULATION RESULTS AND DISCUSSION

Based on a lumped propagation model [39], we perform numerical simulations to reveal the underlying dynamics of the morphology-controllable ultrafast fiber laser. The simulation starts from a low-intensity noise pulse, and the light field is multiplied by relevant matrices when pulses pass through fiber components. After one circulation, the resulted pulse is used as the input of the next round trip until the light field becomes self-consistent. Pulse propagation in fibers is modeled by the generalized nonlinear Schrödinger equation [10,37,40]:

$$\frac{\partial u}{\partial z} = -i\frac{\beta_2}{2}\frac{\partial^2 u}{\partial t^2} + i\gamma|u|^2u + \frac{(g - \alpha)}{2}u + \frac{g}{2\Omega_g^2}\frac{\partial^2 u}{\partial t^2}, \quad (3)$$

where  $u$  is the slowly varying envelope of the pulse;  $z$  and  $t$  correspond to the propagation distance and time, respectively.  $\beta_2$  is the second-order dispersion coefficient,  $\gamma$  is the cubic refractive nonlinearity of the fiber,  $g$ ,  $\alpha$ , and  $\Omega_g$  are the saturable gain, loss of the fiber, and gain bandwidth, respectively. For the SMF,  $g=0$ , and for the EDF,  $g=g_0 \exp(-E_p/E_s)$  [41], where  $g_0$ ,  $E_p$ , and  $E_s$  are the small-signal gain coefficient, pulse energy, and gain saturation energy, respectively. As the pressure applied on the TMF will introduce an extra loss of about 3 dB, the filtering effect can be expressed as  $F=[0.5+0.5\cos(2\pi\Delta n_{\text{eff}}L/\lambda)]/2$  by assuming the two modes have the same intensity.

The nonlinear Schrödinger equation is solved by the predictor-corrector split-step Fourier technique [42], and the CNT SA is modeled by  $T=0.42-0.06/[1+P_{(\tau)}/P_{\text{sat}}]$ , where  $P_{(\tau)}$  is the instantaneous pulse power and  $P_{\text{sat}}$  is the saturable power. We use the following parameters to match the experimental conditions:  $\Delta n_{\text{eff}}=6.2\times 10^{-4}$ ,  $c=3\times 10^8$  m/s,  $n=1.46$ ,  $\alpha=0.02$  dB/km, and  $P_{\text{sat}}=8$  W. According to the measured output powers,  $E_s$  values are 11, 22, and 26 pJ for the dual-color pulse, the narrowband pulse, and the broadband pulse, respectively. For the EDF,  $g_0=13.5$  dB/m,  $\Omega_g=20$  nm,  $\gamma=4.2\times 10^{-3}$  W $^{-1}$ m $^{-1}$ , and  $\beta_2=25.48$  ps $^2$ /km; for the SMF,  $\gamma=1.3\times 10^{-3}$  W $^{-1}$ m $^{-1}$  and  $\beta_2=-21.95$  ps $^2$ /km. The lengths of the EDF, the SMF, and the TMF are 3.5,

3.22, and 1.5 m, respectively. The dispersion and nonlinear parameters of the TMF are the same as those of the SMF for simplicity.

By introducing the filtering effect with the transmission dip located at the central spectrum of the initial pulse, a stable dual-color synchronized pulse can be formed in the cavity after 200 circulations. As shown in Figs. 4(a) and 4(b), two spectra have a separation of 2.71 nm with a 3-dB bandwidth of 0.39 nm. The simulated pulse profile and its AC trace show multipeak structures, which are similar to the experimental observation in Fig. 2. The dual-color synchronized pulse can be regarded as an alternative type of soliton that maintains its nature during the whole evolution process. Its formation relies on three key factors. First, the spectral-filtering effect results in the dual-color operation of the fiber laser. Second, the net group-delay dispersion must be trimmed to the near-zero dispersion regime to realize synchronization of the dual-color pulses. Third, despite the small residual cavity dispersion, the CNT SA forces the pulse at two wavelengths to overlap, as its transmission is proportional to the pulse intensity. Moreover, when the multipeak structure is formed, the CNT SA suppresses the side lobes, which stabilizes the phase locking of two spectra. In comparison with a twin-branch optical parametric amplification

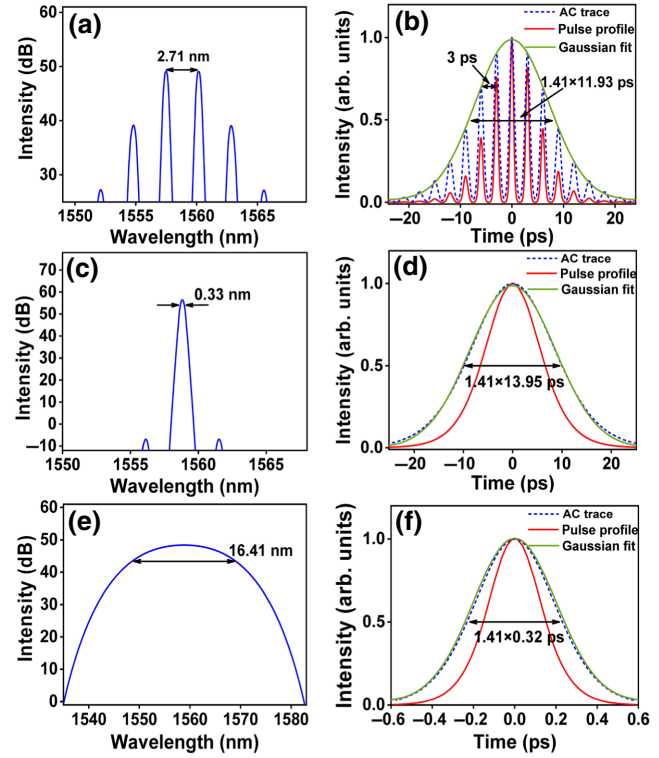


FIG. 4. Simulation results of optical spectra, pulse profiles, and AC traces. (a),(b) Dual-color synchronized pulses; (c),(d) narrowband picosecond pulses; (e),(f) broadband stretched pulses.

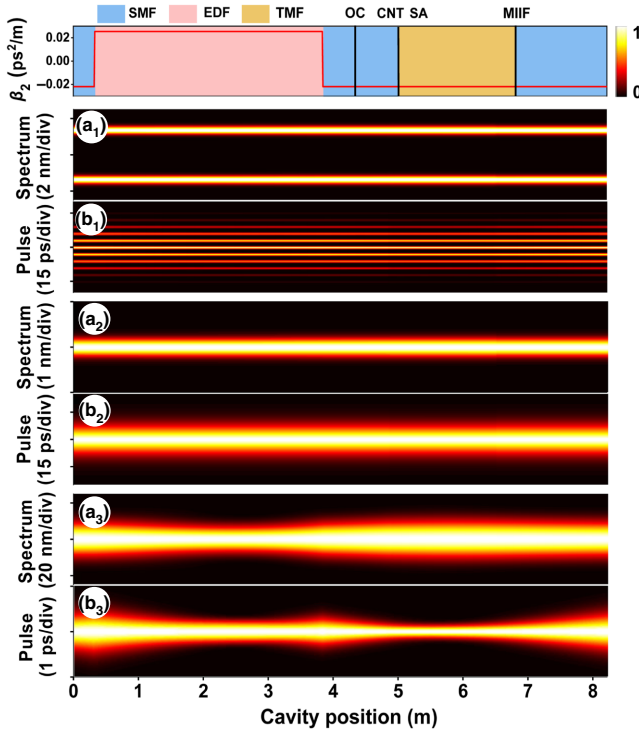


FIG. 5. Intracavity evolution of normalized dual-color synchronized pulses, narrowband pulses, and broadband stretched pulses. (a<sub>1</sub>)–(a<sub>3</sub>) Spectra; (b<sub>1</sub>)–(b<sub>3</sub>) pulses. Upper panel shows dispersion parameters and components versus cavity position.

setup fed by one seed source [43,44], the dual-color synchronized pulses in the fiber laser have the same optical path and repetition rate. Thus, they are expected to possess the same carrier-envelope phase, which may facilitate the generation of phase-locked ultrafast THz pulses with a difference-frequency generation scheme.

When the transmission peak of the filter is tuned to the central wavelength of the initial pulse, a narrowband picosecond pulse is achieved in the simulation. The 3-dB bandwidth is 0.33 nm, and the pulse width is 13.95 ps using Gaussian fitting [Figs. 4(c) and 4(d)]. By removing the spectral filter, a stretched pulse is formed, possessing a 3-dB bandwidth of 16.41 nm and duration of 0.32 ps [Figs. 4(e) and 4(f)]. The numerical results are in good agreement with the experimental observations, validating that the proposed MIIF could control the morphology of ultrashort pulses.

The dynamic evolution of these types of pulses along the cavity is shown in Fig. 5. The intensities are normalized at each cavity position to give a clear comparison of pulse duration and spectral width. In a single round trip, the pulses first propagate through a section of the SMF. After that, the pulses are amplified by the EDF, outputted by the coupler, and then sharpened by the CNT SA. Due to the spectral-filtering effect, dual-color synchronized pulses [Fig. 5(a<sub>1</sub>)] and narrowband pulses [Fig. 5(a<sub>2</sub>)]

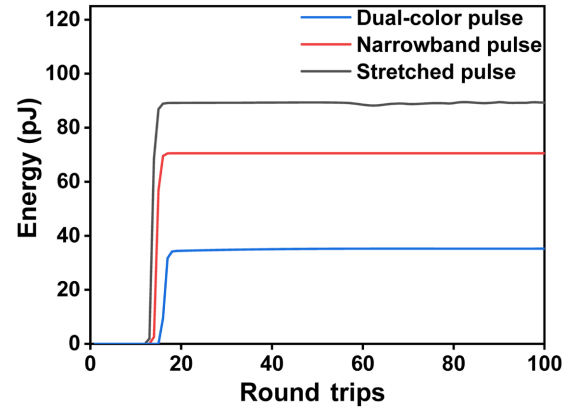


FIG. 6. Energy evolution of dual-color synchronized pulse, narrowband pulse, and broadband stretched pulse versus roundtrips.

are confined in the frequency domain, and their durations [Figs. 5(b<sub>1</sub>) and 5(b<sub>2</sub>)] remain nearly unchanged inside the cavity, which is attributed to the limited bandwidth and intensity of the pulses. It should be noted that the subpulse separation of the dual-color pulse packet is fixed, which results from constant-wavelength spacing of the dual-color pulse. However, the broadband stretched pulse [Figs. 5(a<sub>3</sub>) and 5(b<sub>3</sub>)] varies significantly along the fiber laser, i.e., the bandwidth and duration span from 12.78 to 17.65 nm and 0.73 to 0.26 ps, respectively. In this case, the chromatic dispersion and fiber nonlinearity dominate the breathing behavior [45].

Attributed to the saturable absorption effect, the three types of pulses follow a similar minimum-loss principle to that in the fiber laser, as illustrated in Fig. 6. Affected by the MIIF, the laser evolves from the same low-intensity noise pulse to different morphologies to minimize transmission loss, and thus, maximize gain extraction. For example, to minimize the saturable loss, the dual-color pulse tends to operate in the synchronous state with a multipulse structure [Fig. 5(b<sub>1</sub>)], while the stretched pulse reaches its maximum intensity and minimum duration near the CNT SA [Fig. 5(b<sub>3</sub>)]. Compared with that of the dual-color synchronized pulse and narrowband pulse, the influence of fiber dispersion and the nonlinear effect are stronger for the stretched pulse, which results in different build-up times to the steady states.

## V. CONCLUSION

We demonstrate a hybrid-structure ultrafast fiber laser with the capability of producing switchable dual-color synchronized pulses, narrowband picosecond pulses, and broadband femtosecond pulses by manipulating the transverse modes of the TMF. Benefiting from the near-zero dispersion of the cavity, the dual-color pulses operate in a synchronous state, emitting trains of wave packets with

subpulse repetition rates up to about 0.5 THz. Due to the saturable absorption effect, the laser follows from the minimum-loss principle that the pulse evolves to the special temporal profile [46], i.e., the dual-color pulses are inclined to form multiple peaks in the pulse packet as the higher intensity corresponds to a lower loss inside the laser cavity. This result covers the gap between transverse-mode modulation and a spectral-filtering effect, providing a simple and effective approach for controlling pulse morphology and facilitating different applications.

## ACKNOWLEDGMENTS

This work is supported by the National Key R&D Program of China (Grant No. 2017YFA0303800), the National Natural Science Foundation of China (Grants No. 11874300 and No. 61805277), the Fundamental Research Funds for the Central Universities (Grant No. 3102019JC008), and the Natural Science Foundation of Shaanxi Province (Grants No. 2021JC-09 and 2019JQ-447).

- 
- [1] F. Wang, A. G. Rozhin, V. Scardaci, Z. Sun, F. Hennrich, I. H. White, W. I. Milne, and A. C. Ferrari, Wideband-tunable, nanotube mode-locked, fibre laser, *Nat. Nanotechnol.* **3**, 738 (2008).
- [2] Z. Sun, T. Hasan, F. Torrisi, D. Popa, G. Privitera, F. Wang, F. Bonaccorso, D. M. Basko, and A. C. Ferrari, Graphene mode-locked ultrafast laser, *ACS Nano* **4**, 803 (2010).
- [3] Q. Bao, H. Zhang, Y. Wang, Z. Ni, Y. Yan, Z. X. Shen, K. P. Loh, and D. Y. Tang, Atomic-layer graphene as a saturable absorber for ultrafast pulsed lasers, *Adv. Funct. Mater.* **19**, 3077 (2009).
- [4] M. E. Fermann and I. Hartl, Ultrafast fibre lasers, *Nat. Photonics* **7**, 868 (2013).
- [5] Z. He, Y. Du, C. Zeng, B. Jiang, D. Mao, Z. Sun, and J. Zhao, Soliton metamorphosis dynamics in ultrafast fiber lasers, *Phys. Rev. A* **103**, 053516 (2021).
- [6] L. E. Nelson, D. J. Jones, K. Tamura, H. A. Haus, and E. P. Ippen, Ultrashort-pulse fiber ring lasers, *Appl. Phys. B* **65**, 277 (1997).
- [7] M. A. Solodyankin, E. D. Obraztsova, A. Lobach, A. I. Chernov, A. V. Tausenev, V. I. Konov, and E. M. Dianov, Mode-locked 1.93um thulium fiber laser with a carbon nanotube absorber, *Opt. Lett.* **33**, 001336 (2008).
- [8] K. Tamura, E. P. Ippen, and H. A. Haus, Pulse dynamics in stretched pulse fiber lasers, *Appl. Phys. Lett.* **67**, 158 (1995).
- [9] K. Tamura, E. P. Ippen, H. A. Haus, and L. E. Nelson, 77-fs pulse generation from a stretched-pulse mode-locked all-fiber ring laser, *Opt. Lett.* **18**, 001080 (1993).
- [10] F. O. Ilday, J. R. Buckley, W. G. Clark, and F. W. Wise, Self-similar Evolution of Parabolic Pulses in a Laser, *Phys. Rev. Lett.* **92**, 213902 (2004).
- [11] T. Lei, C. H. Tu, F. Y. Lu, Y. X. Deng, and E. B. Li, Numerical study on self-similar pulses in mode-locking fiber laser by coupled Ginzburg-Landau equation model, *Opt. Express* **17**, 000585 (2009).
- [12] L. M. Zhao, D. Y. Tang, X. A. Wu, and H. Zhang, Dissipative soliton generation in Yb-fiber laser with an invisible intracavity bandpass filter, *Opt. Lett.* **35**, 002756 (2010).
- [13] P. Grelu and N. Akhmediev, Dissipative solitons for mode-locked lasers, *Nat. Photonics* **6**, 84 (2012).
- [14] C. K. Ha, K. S. Lee, D. Kwon, and M. S. Kang, Widely tunable ultra-narrow-linewidth dissipative soliton generation at the telecom band, *Photonics Res.* **87**, 1100 (2020).
- [15] D. Y. Tang and L. M. Zhao, Generation of 47-fs pulses directly from an erbium-doped fiber laser, *Opt. Lett.* **32**, 000041 (2007).
- [16] Y. Wei, B. Li, X. Wei, Y. Yu, and K. K. Y. Wong, Ultrafast spectral dynamics of dual-color soliton intracavity collision in a mode-locked fiber laser, *Appl. Phys. Lett.* **112**, 081104 (2018).
- [17] Z. Y. Yan, X. H. Li, Y. L. Tang, P. P. Shum, X. Yu, Y. Zhang, and Q. J. Wang, Tunable and switchable dual-wavelength Tm-doped mode-locked fiber laser by nonlinear polarization evolution, *Opt. Express* **23**, 004369 (2015).
- [18] L. Yun, X. M. Liu, and D. Mao, Observation of dual-wavelength dissipative solitons in a figure-eight erbium-doped fiber laser, *Opt. Express* **20**, 020992 (2012).
- [19] H. Zhang, D. Y. Tang, X. Wu, and L. M. Zhao, Multi-wavelength dissipative soliton operation of an erbium-doped fiber laser, *Opt. Express* **17**, 012692 (2009).
- [20] J. Peng and H. Zeng, Experimental Observations of Breathing Dissipative Soliton Explosions, *Phys. Rev. Appl.* **12**, 034052 (2019).
- [21] N. Akhmediev, J. M. Soto-Crespo, M. Grapinet, and P. Grelu, Dissipative soliton interactions inside a fiber laser cavity, *Opt. Fiber. Technol.* **11**, 209 (2005).
- [22] G. Q. Hu, Y. L. Pan, X. Zhao, S. Y. Yin, M. Zhang, and Z. Zheng, Asynchronous and synchronous dual-wavelength pulse generation in a passively mode-locked fiber laser with a mode-locker, *Opt. Lett.* **42**, 004942 (2017).
- [23] H. Q. Qin, X. S. Xiao, P. Wang, and C. X. Yang, Observation of soliton molecules in a spatiotemporal mode-locked multimode fiber laser, *Opt. Lett.* **43**, 001982 (2018).
- [24] T. Wang, F. Shi, Y. Huang, J. Wen, Z. Luo, F. Pang, T. Wang, and X. Zeng, High-order mode direct oscillation of few-mode fiber laser for high-quality cylindrical vector beams, *Opt. Express* **26**, 011850 (2018).
- [25] L. G. Wright, D. N. Christodoulides, and F. W. Wise, Spatiotemporal mode-locking in multimode fiber lasers, *Science* **358**, 94 (2017).
- [26] U. Teğin, B. Rahmani, E. Kakkava, D. Psaltis, and C. Moser, Single-mode output by controlling the spatiotemporal nonlinearities in mode-locked femtosecond multimode fiber lasers, *Adv. Photonics* **2**, 056005 (2020).
- [27] Y. Ding, X. Xiao, K. Liu, S. Fan, X. Zhang, and C. Yang, Spatiotemporal Mode-Locking in Lasers with Large Modal Dispersion, *Phys. Rev. Lett.* **126**, 093901 (2021).
- [28] D. Mao, M. K. Li, Z. W. He, and X. Q. Cui, Optical vortex fiber laser based on modulation of transverse modes in two mode fiber, *APL Photonics* **4**, 060801 (2019).
- [29] D. Mao, Z. He, H. Lu, M. Li, W. Zhang, X. Cui, B. Jiang, and J. Zhao, All-fiber radially/azimuthally polarized lasers based on mode coupling of tapered fibers, *Opt. Lett.* **43**, 001590 (2018).

- [30] Y. Zhou, A. Wang, C. Gu, B. Sun, L. Xu, F. Li, D. Chung, and Q. Zhan, Actively mode-locked all fiber laser with cylindrical vector beam output, *Opt. Lett.* **41**, 000548 (2016).
- [31] J. Wang, R. Chen, J. Yao, H. Ming, A. Wang, and Q. Zhan, Random Distributed Feedback Fiber Laser Generating Cylindrical Vector Beams, *Phys. Rev. Appl.* **11**, 044051 (2019).
- [32] J. E. Antonio-Lopez, A. Castillo-Guzman, D. A. May-Arrioja, R. Selvas-Aguilar, and P. LiKamWa, Tunable multimode-interference bandpass fiber filter, *Opt. Lett.* **35**, 000324 (2010).
- [33] R. Chen, J. Wang, X. Zhang, A. Wang, H. Ming, F. Li, D. Chung, and Q. Zhan, High efficiency all-fiber cylindrical vector beam laser using a long-period fiber grating, *Opt. Lett.* **43**, 000755 (2018).
- [34] Y. Zhao, Y. Liu, C. Zhang, L. Zhang, G. Zheng, C. Mou, J. Wen, and T. Wang, All-fiber mode converter based on long-period fiber gratings written in fewmode fiber, *Opt. Lett.* **42**, 004708 (2017).
- [35] Y. H. Zhao, Y. Q. Liu, L. Zhang, C. Y. Zhang, J. X. Wen, and T. Y. Wang, Mode converter based on the long-period fiber gratings written in the two-mode fiber, *Opt. Express* **24**, 6186 (2016).
- [36] A. M. Vengsarkar, P. Lemaire, J. B. Judkins, and V. Bhatia, Long-period fiber gratings as band-rejection filters, *J. Lightwave. Technol.* **14**, 58 (1996).
- [37] D. Mao, X. M. Liu, Z. P. Sun, D. D. Han, G. X. Wang, and F. Q. Wang, Flexible high-repetition-rate ultrafast fiber laser, *Sci. Rep.* **3**, 3223 (2013).
- [38] See the Supplemental Material at <http://link.aps.org/supplemental/10.1103/PhysRevApplied.16.034045> for more detailed discussions. Part 1 shows the frequency-resolved optic gating trace of dual-color synchronized pulses and radio-frequency spectra of three types of pulses. Part 2 demonstrates typical operation states of dual-color synchronized pulses. Part 3 illustrates the vector states of dual-color synchronized pulses. Part 4 shows the central-wavelength tunability of narrowband pulses.
- [39] D. Y. Tang, L. M. Zhao, B. Zhao, and A. Q. Liu, Mechanism of multisiton formation and soliton energy quantization in passively mode-locked fiber lasers, *Phys. Rev. A.* **72**, 043816 (2005).
- [40] G. P. Agrawal, *Nonlinear Fiber Optics*, 4th ed. (Academic Press, New York, 2006).
- [41] D. Y. Tang, H. Zhang, L. M. Zhao, and X. Wu, Observation of High-Order Polarization-Locked Vector Solitons in a Fiber Laser, *Phys. Rev. Lett.* **101**, 153904 (2008).
- [42] A. Bednyakova and S. K. Turitsyn, Adiabatic Soliton Laser, *Phys. Rev. Lett.* **114**, 113901 (2015).
- [43] A. Baltuska, T. Fuji, and T. Kobayashi, Controlling the Carrier-Envelope Phase of Ultrashort Light Pulses with Optical Parametric Amplifiers, *Phys. Rev. Lett.* **88**, 133901 (2002).
- [44] A. Sell, A. Leitenstorfer, and R. Huber, Phase-locked generation and field-resolved detection of widely tunable terahertz pulses with amplitudes exceeding 100 MV/cm, *Opt. Lett.* **33**, 002767 (2008).
- [45] W. He, M. Pang, C. R. Menyuk, and P. S. J. Russell, Sub-100-fs 1.87 GHz mode-locked fiber laser using stretched-soliton effects, *Optica* **3**, 001366 (2016).
- [46] L. G. Wright, P. Sidorenko, H. Pourbeyram, Z. M. Ziegler, A. Isichenko, B. A. Malomed, C. R. Menyuk, D. N. Christodoulides, and F. W. Wise, Mechanisms of spatiotemporal mode-locking, *Nat. Phys.* **16**, 565 (2020).